

PCCP

Accepted Manuscript



This is an *Accepted Manuscript*, which has been through the Royal Society of Chemistry peer review process and has been accepted for publication.

Accepted Manuscripts are published online shortly after acceptance, before technical editing, formatting and proof reading. Using this free service, authors can make their results available to the community, in citable form, before we publish the edited article. We will replace this *Accepted Manuscript* with the edited and formatted *Advance Article* as soon as it is available.

You can find more information about *Accepted Manuscripts* in the [Information for Authors](#).

Please note that technical editing may introduce minor changes to the text and/or graphics, which may alter content. The journal's standard [Terms & Conditions](#) and the [Ethical guidelines](#) still apply. In no event shall the Royal Society of Chemistry be held responsible for any errors or omissions in this *Accepted Manuscript* or any consequences arising from the use of any information it contains.

Quantum dynamics of the pick up process of atoms by superfluid helium nanodroplets. The Ne + (⁴He)₁₀₀₀ system

Arnau Vilà^a, Miguel González^{a,*} and Ricardo Mayol^{b,*}

^a Departament de Química Física i IQTC, Universitat de Barcelona, c/ Martí i Franquès, 1, 08028 Barcelona, Spain.

^b Departament d'Estructura i Constituents de la Matèria, Universitat de Barcelona, c/ Martí i Franquès, 1, 08028 Barcelona, Spain.

Abstract

The capture dynamics of a Ne atom by a superfluid helium nanodroplet ((⁴He)_{N=1000}; $T=0.37$ K), $\text{Ne} + (^4\text{He})_N \rightarrow \text{Ne}@(^4\text{He})_N$, was investigated using a quantum approach (TDDFT (helium) + quantum wave packet (Ne)) at zero angular momentum and a rather wide range of Ne atom initial mean velocities ($\langle v_0 \rangle$: 90-1300 m/s). This is probably the first quantum dynamics study focused on the pick up process and the evolution of the dopant inside the nanodroplet and the second more detailed investigation on this topic. For $\langle v_0 \rangle \geq 210$ m/s and above the atom is always captured, but for lower velocities the probability of capture is somewhat below the unity and decreases as $\langle v_0 \rangle$ diminishes. The main energy exchange begins with the collision of the atom with the nanodroplet surface, and the excess of energy placed in the doped nanodroplet is progressively released by evaporation of a small amount of ⁴He atoms. Once the atom has entered into the nanodroplet its mean position follows an oscillatory trajectory, due to multiple sequential collisions with the inner surface of the nanodroplet, and its mean velocity reaches values which are below the Landau's critical velocity. This probably corresponds to the general behavior for nanodroplets with a bulk-like region when moderate collision energies (i.e., similar to the ones considered here) are involved.

In the future we hope to investigate the influence of angular momentum on the mechanism of the pick up process, using the same quantum dynamics method.

Keywords: helium nanodroplet, impurity, Ne atom, pick up, capture, theory, quantum dynamics, time dependent DFT, wave packet, velocity, energy, helium vaporization.

Tables: 2 **Figures:** 6.

† **Electronic Supplementary Information (ESI) available.** See DOI:

Tables: Table S1. Cartesian grids and propagation time steps. Table S2. Spatial separation of the Cartesian grids. Table S3. Final propagation times. **Figures:** Figure S1. Maxwell velocity distribution of the Ne atom at $T = 300$ K. Figure S2. Snapshots showing the temporal evolution of the probability density of the Neon atom wave packet in momentum representation. Figure S3. Trajectories of the mean values of the Ne atom velocity and position as function of $\langle v_0 \rangle$. **Movies:** Movie 1. Time evolution of the Ne atom z-axis wave packet in coordinate and momentum representations. Time evolution of the helium density along the z-axis and in the xz-plane. Movie 2. As movie 1 but for $\langle v_0 \rangle = 500$ m/s. Movie 3. As movie 1 but for $\langle v_0 \rangle = 800$ m/s.

* Corresp. authors: miguel.gonzalez@ub.edu; Fax: +34934021231; ricardo.mayol@ub.edu; Fax: +34934037063.

(Revised manuscript submitted to Phys. Chem. Chem. Phys., 7-11-2015)

1. INTRODUCTION

The investigation of the structure, energy and dynamics of superfluid helium nanodroplets ($(^4\text{He})_N$; $T=0.37\text{ K}$) is a well-established research area in physics.^{1,2} From a fundamental point of view these nanodroplets have a large interest because of their intermediate size, which essentially ranges from clusters to the bulk liquid, which allows to obtain a deep insight into the properties of quantum fluids and on the manner their properties evolve as the system size does. Moreover, helium nanodroplets can be used as low temperature matrices for high resolution spectroscopic studies, due to chemically inert character of He and the superfluid behavior of liquid ^4He below $T=2.17\text{ K}$.^{3,4,5}

Since the first study of a chemical reaction in a helium nanodroplet,⁶ the contributions reported so far on chemical reactivity in helium nanodroplets have been important (see, e.g., refs. 7, 8, 9, 10 and 11, and the references cited therein), even though the strength of these efforts is not comparable to those performed in the context of the physical studies. Lately, however, it seems that the chemical interest on this quantum fluid has increased significantly; and this probably results from the new possibilities offered by helium nanodroplets in the synthesis of new chemical species. Thus, they allow obtaining species that would not be stable in gas phase as, e.g., some metallic nanoclusters^{12,13,14} and nanowires.^{15,16}

Furthermore, some efforts have also been addressed to explore the chemical reaction dynamics in the $(^4\text{He})_N$ quantum fluid,^{1,17} both experimental (e.g., photodissociation of alkyl iodides,^{18,19,20} bimolecular reactions involving metals, $\text{Mg} + \text{O}_2$,²¹ $\text{Al} + \text{O}_2$, H_2O ,⁸ $\text{Ba} + \text{N}_2\text{O}$,⁶ etc.) and theoretically (photodissociation of $\text{Cl}_2(\text{B})$ in superfluid^{10,11} and non-superfluid²² helium nanodroplets). Although the main interest of our group in this context focuses on the theoretical study of the reaction dynamics inside helium nanodroplets, before studying these processes we consider that it is very interesting to characterize the pick up (or capture) process of chemical species by superfluid $(^4\text{He})_N$, which corresponds to the previous stage needed for studying chemical

reactions inside nanodroplets. The dopant species in addition to be involved as a reactant, of course, can also be used as a probe in order to extract information about the nanodroplets.

It was in molecular beam experiments involving Ne and clusters of He where it was clearly shown for the first time that helium was able to capture atomic species.²³ Helium nanodroplets can capture a very wide range of atomic and molecular species, e.g., Ar, Kr, Xe, H₂O, and SF₆,²⁴ Ar_n,²⁵ Kr_n,²⁶ transition metal atoms (Cr_n,²⁷ Cu_n,²⁸ ..), radical species from organic molecules (ethyl radical),²⁹ aromatic organic molecules and related species (anthracene, pyrromethene, porphyrin derivatives),³⁰ fullerene and small molecules (C₆₀(H₂O)_n, C₆₀(NH₃)_n and C₆₀(CO₂)_n).³¹ etc.

In spite of its interest and the experimental efforts (see, e.g., refs. 23, 32 and 33) the information available about the dynamics of the capture process is still quite limited. The first attempt to describe the quantum scattering dynamics from helium nanodroplets goes back to 1988,³⁴ and the first analysis, from a quantum perspective, of the motion of impurities inside these nanodroplets are from the late 1990s.^{35,36} More detailed many-body studies were reported more recently on the quantum scattering from helium nanodroplets and surfaces.^{37,38,39} However, the first realistic simulation of the penetrating collision of an atom (Cs) with a helium nanodroplet has been obtained only very recently.⁴⁰

Therefore, the ability of nanodroplets to capture almost any chemical species is of crucial importance and has been the main motivation of this work. Thus, we have theoretically investigated the quantum dynamics of the pick up process of a Ne atom by a superfluid helium nanodroplet of 1000 helium atoms ($N=1000$), $\text{Ne} + ({}^4\text{He})_N \rightarrow \text{Ne}@({}^4\text{He})_N$, exploring a rather wide range of velocities (90-1300 m/s), which are representative of those typical in a pick up experimental chamber. To the best of our knowledge this is the first quantum dynamics study carried out specifically on the pick up process and the motion of the dopant inside the nanodroplet and the second more detailed contribution on this interesting subject.

The superfluid helium nanodroplet was described by the time dependent density functional theory (TDDFT) and the Ne atom was described quantum-mechanically using a wave packet, i.e., following the same hybrid approach proposed by us recently.¹⁰ Due to the high computational effort needed for a quantum description of the capture problem, in this first study we have restricted the analysis to the case of zero total angular momentum (head-on collisions).

The Ne + (⁴He)_N system was chosen primarily by the fact that, among all the analogous systems in which we can consider the capture of a noble gas atom, i.e., Rg + (⁴He)_N → Rg@(⁴He)_N (Rg: He, Ne, Ar, Kr, Xe, Rn), and regardless of helium, it is the one that, due to the small mass of neon, is more likely to present a quantum behavior. Moreover and as a curiosity, it was in collisions involving Ne and clusters of He where the capture process was clearly evident for the first time.²³

This paper has the following structure: the theoretical methods employed are concisely explained in section II; the description and analysis of the most important results achieved is given in section III; and to finish the summary and conclusions are reported in section IV. Supplementary useful information has been included in the Electronic Supplementary Information (ESI) document associated to this contribution.

2. THEORETICAL METHODS

The study of the dynamics of the pick up process has been carried using a quantum treatment of the system, i.e., the impinging Ne atom and the helium nanodroplet, following an analogous theoretical approach as that proposed by us recently to describe the photodissociation of diatomic molecules in helium nanodroplets.¹⁰ Thus, we have combined one of the main theoretical procedures employed to describe rather large systems of bosonic liquid helium (TDDFT; from hundred to thousands of atoms) and a usual method in gas phase time dependent quantum reaction dynamics (quantum wave packets (WP)), to account for the evolution of the helium nanodroplet and the neon atom, respectively. This strategy allows us to investigate relatively big nanodroplets, in

this way making possible the highly desirable interaction with the experiments.

For the TDDFT description of the superfluid liquid helium, we have used the so-called Orsay-Trento phenomenological functional,⁴¹ neglecting the backflow term and the non-local contribution to the helium correlation energy for computational reasons.^{10,11,40} Major numerical difficulties result when these terms are taken into account, because exceptionally small integration steps are required. It is worth noting here that the theoretical study of the dynamics of processes involving superfluid helium nanodroplets and atomic or molecular species has only become possible quite recently and this approach has been employed in all cases, leading to a rather good agreement with the experimental findings.^{42,43,44} The Orsay-Trento functional is characterized via the $\mathcal{E}_c[\rho_{He}]$ term in equation 1b, which in the present study corresponds to the potential and correlation energy density of superfluid helium.

Since in this first study we only consider the situation of zero angular momentum, only a one-dimensional (z-axis) standard quantum wave packet dynamics is needed to describe the evolution of the dopant Ne atom. This is equivalent to treat the x and y neon degrees of freedom classically, and so they are represented in the total spatial wave function of Ne as a Dirac delta distribution, i.e., $\Psi_{Ne}(\mathbf{r}_{Ne}) \cong \phi_{Ne}(z_{Ne})\delta(x_{Ne})\delta(y_{Ne})$. Consequently, we have not paid attention neither on the effects of the natural spreading of the wave packet during the approach of the Ne atom to the nanodroplet, nor on the natural zero point motion inside the droplet in the (x, y) perpendicular directions. These effects would merely produce small perturbations to the physics of the pick-up process,⁴⁵ in which we are really interested, but largely increasing the computational cost of the calculations.

A detailed description of the TDDFT+WP method for doped (X_2 diatomic molecules) superfluid helium can be found in our previous work,¹⁰ and here we will report the main equations and particularities of the present study. For the modeling of the Ne + (^4He)_N system, the quantum action in terms of the effective complex wave function of (^4He)_N, $|\Psi_{He}(R_{He}, t)|^2 \equiv \rho_{He}(R_{He}, t)$,

and the z-axis wave packet of Ne, $\phi_{Ne}(z_{Ne}, t)$, read as:

$$\begin{aligned} \mathcal{A}[\Psi_{He}, \phi_{Ne}] = & \int dt \left\{ E[\Psi_{He}, \phi_{Ne}] - i\hbar \int d\mathbf{R}_{He} \Psi_{He}^*(\mathbf{R}_{He}) \frac{\partial}{\partial t} \Psi_{He}(\mathbf{R}_{He}) \right. \\ & \left. - i\hbar \int dz_{Ne} \phi_{Ne}^*(z_{Ne}) \frac{\partial}{\partial t} \phi_{Ne}(z_{Ne}) \right\} \end{aligned} \quad (1a)$$

where E is the total energy of the system that is given by the following expression:

$$\begin{aligned} E[\Psi_{He}, \phi_{Ne}] = & \frac{\hbar^2}{2m_{He}} \int d\mathbf{R}_{He} |\nabla \Psi_{He}|^2 + \int d\mathbf{R}_{He} \mathcal{E}_c[\rho_{He}] \\ & + \int d\mathbf{R}_{He} \int dz_{Ne} V_{He-Ne}(z_{Ne}, \mathbf{R}_{He}) \rho_{He}(\mathbf{R}_{He}) |\phi_{Ne}(z_{Ne})|^2 \\ & - \frac{\hbar^2}{2m_{Ne}} \int dz_{Ne} \phi_{Ne}^*(z_{Ne}) \frac{\partial^2}{\partial z_{Ne}^2} \phi_{Ne}(z_{Ne}) \end{aligned} \quad (1b)$$

The He-Ne diatomic potential energy curve has been taken from the *ab initio* coupled-cluster quantum chemical calculations reported in ref. 46, where a large basis set was used; and the helium nanodroplet-neon atom interaction has been described according to the common pairwise approach.

To obtain the equations of motion governing the time evolution of helium and the Ne atom, the quantum action (eq. 1a) has to be minimized by performing variations of the wave functions Ψ_{He} and ϕ_{Ne} . This leads to a pair of coupled non-linear Schrödinger-like equations:

$$i\hbar \frac{\partial}{\partial t} \Psi_{He}(\mathbf{R}_{He}) = \left[-\frac{\hbar^2}{2m_{He}} \nabla^2 + \int dz_{Ne} V_{He-Ne}(z_{Ne}, \mathbf{R}_{He}) |\phi_{Ne}(z_{Ne})|^2 + \frac{\delta \mathcal{E}_c[\rho_{He}]}{\delta \rho_{He}} \right] \Psi_{He}(\mathbf{R}_{He}) \quad (2a)$$

$$i\hbar \frac{\partial}{\partial t} \phi_{Ne}(z_{Ne}) = \left[-\frac{\hbar^2}{2m_{Ne}} \frac{\partial^2}{\partial z_{Ne}^2} + \int d\mathbf{R}_{He} V_{He-Ne}(z_{Ne}, \mathbf{R}_{He}) \rho_{He}(\mathbf{R}_{He}) \right] \phi_{Ne}(z_{Ne}) \quad (2b)$$

Equations 2a and 2b have been discretized using Cartesian grids. We have employed different grids (depending of the initial velocity of the Ne atom) to properly account for the physics

of each case; since the spacing in the coordinate grid is proportional to the maximum value of the conjugated momentum grid. The characteristics of the different grids used are given in Tables S1 and S2.

The time propagation has been performed using the Adams predictor-corrector-modifier method,⁴⁷ initiated by a fourth order Runge-Kutta method⁴⁸ (the time step used varied from $3.0 \cdot 10^{-4}$ to $8.0 \cdot 10^{-5}$ ps from 90 to 1300 m/s, respectively). The derivatives for the kinetic energy terms have been calculated in momentum space by means of a Fourier transform using the FFTW package of ref. 49.

In order to absorb the helium density evaporated from the nanodroplet and to avoid non-physical reflections of the helium effective wave function, a quartic negative imaginary potential (NIP) has been introduced in the edges of the grid.⁵⁰ We also applied a NIP to the edges of the Ne grid so as to account for the possibility of rebound of a fraction of the wave packet due to the collision with the nanodroplet. The NIPs have the following expression:

$$V_{\text{NIP}} = -i A \frac{5}{2} \left(\frac{d - d_{\text{NIP}}}{L} \right)^4 \quad (3)$$

for $d > d_{\text{NIP}}$, where the absorption strength (A) is equal to 331.5 and $3315.0 \text{ K } \text{\AA}^{-4}$ for the Ne atom and helium, respectively, the length (L) is equal to 1 \AA , and the location (d_{NIP}) of the NIPs are indicated below. The atomic NIP is placed in the z-axis at 12.1 \AA ($\langle v_0 \rangle = 90\text{-}500 \text{ m/s}$) and 8.8 \AA ($\langle v_0 \rangle = 800\text{-}1300 \text{ m/s}$) with respect to the $(^4\text{He})_{\text{N}}$ surface (nanodroplet radius = 25 \AA). The NIPs for $(^4\text{He})_{\text{N}}$ are located in the z-axis at 13.1 \AA ($\langle v_0 \rangle = 90\text{-}500 \text{ m/s}$) and 9.8 \AA ($\langle v_0 \rangle = 800\text{-}1300 \text{ m/s}$) with respect to the nanodroplet surface, while for the x and y-axis they are at 12.6 \AA ($\langle v_0 \rangle = 90\text{-}500 \text{ m/s}$) and 10.6 \AA ($\langle v_0 \rangle = 800\text{-}1300 \text{ m/s}$).

Concerning the initial conditions for the dynamics, we have considered a pure helium nanodroplet of 1000 ^4He atoms and a minimum uncertainty Gaussian wave packet describing the Ne atom (eq. 4). The wave packet has been centered in the z-axis at $\mu = -35 \text{ \AA}$, which is far enough

from the nanodroplet to consider the situation as asymptotic (Ne-helium interaction energy = -0.065 K). For the width of the wave packet we selected the value $\sigma=0.8 \text{ \AA}$ since this leads to a description of the WP with almost the same number of points in the position and momentum grids.

$$\phi_{Ne}(z_{Ne}, t = 0) = \frac{1}{(2\pi\sigma^2)^{1/4}} e^{-\frac{(z_{Ne}-\mu)^2}{4\sigma^2}} e^{i\frac{p_0}{\hbar}(z_{Ne}-\frac{\mu}{2})} \quad (4)$$

The initial values of the kinetic energy of the impinging Ne atom, the Ne-(He)_N interaction energy and the internal energy (kinetic and potential + correlation) of (He)_N can be seen in Table 1. The numerical parameters defining the Cartesian grids of the Ne atom and helium are given in Tables S1 (including the propagation time steps) and S2, while the final simulated times are reported in Table S3.

3. RESULTS AND DISCUSSION

The process of capture of neon atoms by helium nanodroplets with angular momenta equal to zero (i.e., zero impact parameter, classically) has been studied at several initial mean velocities of Ne ($\langle v_0 \rangle = 90, 120, 210, 300, 500, 800, 1200$ and 1300 m/s). These velocities have been selected in order to account for representative velocities of a Maxwell velocity distribution of Ne atoms at $T = 300 \text{ K}$ (Figure S1), i.e., for rather typical experimental conditions in the pick up chamber. Moreover, instead of proceeding in the usual way (i.e., employing typically one or two wave packets to cover the full interval of velocities of interest), we have considered a set of independent calculations employing wave packets that are centered in representative values of the velocities; since our main goal is centered in the detailed analysis of the microscopic mechanism of the pick up process as a function of the initial velocity.

The simulated times are not the same for all cases (Table S3). With the exception of the two higher velocities we have stopped the calculations at a time around 150-200 ps. This choice is mainly based on physical arguments, which will be clear hereafter, and also due to the high

computational cost of these calculations.

To visualize the dynamical mechanism of the picking up of a Ne atom by a helium nanodroplet, some movies have been prepared, which include the time evolution of the probability density of the Ne atom wave packet in coordinate ($|\phi_{Ne}(z_{Ne})|^2$) and momentum ($|\tilde{\phi}_{Ne}(p_{z_{Ne}})|^2$) representations and the helium density in the z-axis and in the xz-plane (cf. movies 1-3 in the ESI for $\langle v_0 \rangle = 210, 500$ and 800 m/s, respectively). Moreover, Figure 1 shows snapshots of the temporal evolutions of $|\phi_{Ne}(z_{Ne})|^2$ and the helium density at selected times for $\langle v_0 \rangle = 500$ m/s (maximum of the Ne velocity distribution at $T = 300$ K; cf. Figure S1), where it can be seen that $|\phi_{Ne}(z_{Ne})|^2$ is narrower inside the nanodroplet than in the initial wave packet, as a result of helium solvation. Figure S2 shows the analogous representation for $|\tilde{\phi}_{Ne}(p_{z_{Ne}})|^2$.

Leaving out the Ne atom approach to the nanodroplet, three different steps can be identified in the pick up process. The first one corresponds to the penetration of the atom through the nanodroplet surface, which acts as a dynamical potential barrier. Once the Ne atom is inside the nanodroplet its velocity decreases due to the interaction with the helium environment. Then, when the atom velocity reaches a limiting value below the Landau's critical velocity (≈ 58 m/s (0.58 \AA/ps) in superfluid (bulk) helium^{51,52} and also recently observed in nanodroplets with $N \geq 1000$ ⁴²), it remains stable until the atom approaches to the nanodroplet inner surface and bounces back. It should be noted here that, due to the (reasonable) simplifications made in the helium functional to make possible the present calculations, the critical velocity is about 90 m/s.⁴² At this stage of the process the only mechanism of exchanging energy from the moving Ne atom to the nanodroplet is based on the activation of the surface excitation modes. This is a very slow relaxation mechanism that occurs each time the atom reaches the nanodroplet inner surface and because of this we stopped the simulations for computational reasons.

Focusing on the first step of the process, a wide range of different behaviors is found, depending on the initial velocity. For the softer impacts ($\langle v_0 \rangle = 90$ and 120 m/s) some fraction of

the wave packet is reflected during the collision with the nanodroplet. Thus, for the 90 m/s case the 88.0% of the WP is captured while for 120 m/s a value of 98.5% is obtained. The remaining cases have a penetration coefficient of 100%, i.e., all the WP is captured by the nanodroplet. Although a detailed characterization of the dependence of the penetration probability with the initial velocity and the analysis of possible quantum effects as tunnelling, interferences and resonances (quasi bound states) has a significant interest, it is out of the scope of the present paper and we expect to investigate them in a future work.

When the Ne atom collides with the nanodroplet surface, an oscillatory pattern, which increases with the initial velocity, can be observed in both the Ne wave packet probability density and the helium density (cf. Figure 1 and movies 1-3 (ESI)). The dynamical behaviour is essentially the same for the full penetration cases, with only small differences. The wavelength of the helium density oscillations decreases with the initial velocity (collision energy), indicating that the nanodroplets become progressively more excited as $\langle v_0 \rangle$ increases. The formation of a stable solvation shell around the Ne atom is only produced when the nanodroplet is not highly excited, because in the former situation the helium density waves destroy the solvation structures which are permanently being formed and destroyed. Besides, from the evolution of the helium density in the xz-plane it can be seen the very small distortion suffered by the geometry of the nanodroplet. This has been found in other dynamical processes occurring in helium nanodroplets, such as the photodissociation of Cl_2 ^{10,11} and the ionization of heavy atoms,⁵³ where higher energies are involved.

From Figure S2 ($\langle v_0 \rangle = 500$ m/s) and movies 1-3 ($\langle v_0 \rangle = 210, 500$ and 800 m/s, respectively) it can be seen that the Ne wave packet probability density in momentum space moves towards lower momentum values, when the collision with the nanodroplet surface takes place. In all cases, at a certain time, the square modulus of $\text{WP}(p)$ adopts a Gaussian-type shape centered at a particular value of momentum; and this happens when the mean velocity of Ne is below the Landau's critical

velocity.

This means that the square modulus of $WP(r)$ has also a Gaussian profile (the Fourier transform of a Gaussian function is a function of the same type). Therefore, keeping in mind that these wave functions are eigenfunctions (solutions) of an harmonic oscillator problem and in virtue of the Galilean transformation, we infer that $WP(r)$ is placed in a harmonic-like potential moving at constant velocity. This is consistent with the fact that the wave function is placed around the minimum of a moving potential, and so it is locally quadratic, which is also reasonable from a classical point of view, since the force must be zero in the minimum of a potential. Therefore, an almost isotropic distribution of helium must surround the impurity in order to produce such a essentially symmetric potential, as can be confirmed by movies 1-3. Finally, when the Ne atom reaches the nanodroplet inner surface, the momentum wave packet changes passing through the zero value and the sign of the momentum changes.

The mean values are useful in this context and the time evolution of the mean value of the Ne atom position, i.e., $\langle z_{Ne} \rangle$, is plotted in Figure 2. In this and the following figures the temporal evolution of magnitudes associated to $\langle v_0 \rangle = 90$ and 120 m/s cases finishes at $t = 31.1$ and 19.4 ps, respectively, because at these times the NIP begins to absorb the reflected part of the wave packets (which only occurs in these two cases) and then the wave packets are no longer normalized. Besides, it should be noted that here we are mainly interested in the dynamics when the atom is fully captured by the ^4He nanodroplet ($\langle v_0 \rangle = 210$ -1300 m/s).

For $\langle v_0 \rangle = 300$ m/s the calculations show up to three rebounds of $WP(r)$ with the nanodroplet surface. The amplitude of the oscillations does correlate in a simple way with the initial velocity value, and the $\langle v_0 \rangle = 210$ m/s case has lower turning points than the other velocities. It can also be seen that the turning points are not symmetric. Both facts point out how the helium density waves, whose magnitude depends on the initial collision energy, influence the dynamics. This is probably due to the somewhat comparable value of the Ne and He masses ($m_{Ne}/m_{He} \approx 5$). For heavier dopants

a different behavior would be expected.

The temporal evolution of the mean values of the Ne velocity, focusing on the collision and the atomic motion inside the nanodroplet, is presented in Figure 3. For the higher velocities ($\langle v_0 \rangle = 1300, 1200, 800$ and 500 m/s) the deceleration follows, on the overall, almost the same curve and at around $t = 8-9$ ps $\langle v_{\text{Ne}} \rangle$ reaches a minimum whose value decreases with the initial velocity. This minimum is due to a push of the helium density waves that happens when a relatively stable helium solvation shell is formed (cf. movies 1-3). So that, during the process of changing from a slightly asymmetric to a symmetric potential well (quadratic), a small kick to the Ne atom is produced.

This means that the momentum transfer is not unidirectional, as there is also a small momentum transfer from the helium to the Ne atom. This also occurs for $\langle v_0 \rangle = 300$ and 210 m/s but it is less evident, since the excitation of the helium nanodroplet is smaller. For the softer collision conditions ($\langle v_0 \rangle = 90$ and 120 m/s) there is a remarkable acceleration before the penetration of the nanodroplet surface, due to the attractive interaction between the Ne atom and the nanodroplet. This is not observed in the other cases since their velocities are high enough, so that the approaching process is similar to a solid collision.

The evolution of the velocities once the Ne atom is inside the nanodroplet is also shown in Figure 3. For most cases the velocity tends to remain constant during the atom travel through the bulk-like part of the nanodroplet, although some small oscillations are present. This is consistent with the existence of a Landau's critical velocity in helium nanodroplets recently reported experimental and theoretically.⁴² Within the TDDFT level of theory, using the Orsay-Trento functional and neglecting the backflow and correlation alpha terms a value of 90 m/s has been determined. Here we have obtained an analogous result, but with a quantum probe (Ne atom) rather than a classical one as in the theoretical study of ref. 42.

This phenomenon is clearly evident after the first collision with the nanodroplet inner

surface. Each pick up case examined has a different limiting velocity and this arises from the different initial collision conditions (the reason of this behaviour will be explained in the next paragraphs). Once the Ne atom is moving below the Landau's critical velocity, the only possible mechanism to release energy to the nanodroplet results from the excitation of the surface modes (ripples). This may occur every time the atom collides with the nanodroplet inner surface, although we have found that in the examined cases this is not an efficient process. Because of this we decided to finish the calculations, since an oscillating pattern in the $\langle v_{\text{Ne}} \rangle$ vs. time dependence is expected to be present for a very long period of time. Hence, the continuation of the simulations is not expected to give new insights into the physics of the process.

The analysis of the evolution of $\langle v_{\text{Ne}} \rangle$ versus $\langle z_{\text{Ne}} \rangle$ allows us to obtain some more light on the mechanism of the pick up process (Figure 4), paying attention to the different limiting velocities found. This plot corresponds to the representation of the average trajectories in phase space, excepting that the mass of the Ne atom is not multiplying the mean velocity along the z-axis. The dashed line in Figure 4 shows the z value for the pure nanodroplet surface (radius of 25 Å), and from around this point the Ne velocity begins to change, increasing or decreasing depending on the initial velocity.

Two markedly different regions are present, corresponding to the two regimes of the pick up dynamics. The first region presents two straight lines in the $\langle v_{\text{Ne}} \rangle$ versus $\langle z_{\text{Ne}} \rangle$ plot: a horizontal line (constant velocity) that is followed by an oblique line (deceleration). The second line indicates the presence of a friction force of the type $F_f = -b\langle v_{\text{Ne}} \rangle$, resulting from the interaction of Ne with the helium nanodroplet. That is to say, the helium behaves as a conventional fluid as it has also been recently reported by us in a Cl₂ photodissociation quantum study.^{10,11} So that, during the first dynamic regime, there is an important energy release from the Ne atom to the helium nanodroplet (which is particularly important for $\langle v_0 \rangle$ above 120 m/s), with the subsequent rapid decrease of the Ne velocity.

The second $\langle v_{\text{Ne}} \rangle$ vs. $\langle z_{\text{Ne}} \rangle$ region follows after the first region and presents average trajectories with an ellipsoidal-like shape that corresponds to the oscillations of the Ne atom inside the nanodroplet (from the right to left and so on). These phase-orbits are almost closed and each studied case has its own “ellipse”. Excepting the case of $\langle v_0 \rangle = 210$ m/s, whose phase trajectory is slightly different, the others follow a similar pattern. From Figure 4 we can also see that each $\langle v_0 \rangle$ value results in a different $\langle z_{\text{Ne}} \rangle$ value, once the trajectory of the mean values gets into its own ellipsoidal-like motion in phase space and, of course, also results in a different excitation of the nanodroplet (Table 2). A more detailed view of the “ellipses” region is presented in Figure S3.

In the $\langle z_{\text{Ne}} \rangle$ points near the nanodroplet surface there is a net force pointing towards the center due to the non-symmetric solvation of the dopant. Observing the quasi-ellipses, we see that the curvature of the phase-trajectories takes place from a distance of around 10 \AA off the nanodroplet center, independently of the case considered. Therefore, for the Ne atom impurity there is a part of the ${}^4\text{He}_{1000}$ nanodroplet that shows bulk-like character and has a length of about 20 \AA . This would be a sort of measure of the completeness (effective symmetry) of the Ne atom solvation and, of course, we expect that this value will depend on both the helium and the impurity (dopant) considered. In this region, once the atom velocity becomes smaller than the Landau’s critical velocity, it would remain essentially constant if the nanodroplet is not so excited.

From these considerations we can understand better the origin of the different “ellipses” found in the calculations. Disregarding the effects produced by the density waves in liquid helium (excitation), the phase trajectory would begin to become similar to an ellipse when the atom reaches the Landau’s critical velocity, unless this velocity is reached in a “non-bulk” zone of the nanodroplet. This together with the remaining excitation of the nanodroplet will determine the shape of the “ellipse” in each case.

We estimated the excitation energy per helium atom of the nanodroplet at the time when the phase trajectory becomes an “ellipse” by $\Delta e(t) = e(t) - e_{\text{Ne}@}{}^4\text{He}_{1000}}$, where $e \equiv E/N$ is the

energy of the perturbed nanodroplet divided by the number of helium atoms, and $e_{Ne@{}^4He_{1000}}$ is the corresponding ground state energy per helium atom. These energies only correspond to helium, i.e., neither the Ne-helium interaction energy nor the Ne kinetic energy are included (Table 2). Hence, when the Ne atom moves at a constant velocity the excitation of the nanodroplet is not the same for all the cases examined. This would also explain the fact that for the higher initial velocities the “turning points” are closer to the center of the nanodroplet, because there are energetic helium density waves reflecting at the nanodroplet surface and pushing the Ne atom back towards the centre.

To complete the analysis of the pick up process we focused our attention into the evolution of the E/N ratio on time. During the collision of the Ne atom with the nanodroplet external surface the energy exchange from the atom to the nanodroplet begins to occur in an intense way (Figure 5). Besides, for all the $\langle v_0 \rangle$ values the E/N vs. time dependence shows the same behaviour. At the beginning E/N increases (first monotonically and then non-monotonically (“oscillations”)), then reaches a maximum and, finally, decreases with time, due to the evaporation of helium atoms (Figure 6), and tends to a constant value. Structures (“oscillations”) are also evident in Figure 3, when showing the mean value of the Ne velocity vs. time, which is directly related to its kinetic energy.

The asymptotic behaviour of the E/N vs. t curves, i.e., that for the final simulation time, suggests that at around 150-200 ps all the doped nanodroplets are almost relaxed (Figure 5). This time scale is shorter but comparable with that found in the case of the relaxation of nanodroplets of different sizes ($N=50-500$) after the photodissociation of a $Cl_2(B)$ embedded molecule (several hundred picoseconds),⁵⁴ where higher energies are involved.

The E/N value obtained in the asymptote is somewhat greater than that for the nanodroplet at $t=0$ (Figure 5). To clarify this result we have carried out a static calculation of the $Ne@{}^4He_{1000}$ nanodroplet, obtaining a E/N value of -5.35 K, which compares very well with the ≈ -5.33 K value

determined for the asymptotic value, even though there is a little difference ($\approx 1.3\%$) in the number of He atoms of both nanodroplets (cf. Figure 6). Therefore, the E/N change observed in the asymptote is only due to the differences in the initial and final situations (non-doped vs. doped nanodroplets, respectively). Moreover, the E/N value of the asymptote is also similar to the corresponding value of the pure nanodroplet (-5.40 K).

To conclude, we have compared the kinetic energy corresponding to the zero point motion of the Ne atom doping the static nanodroplet with the asymptotic values of the present dynamics study. The asymptotic values of the Ne atom kinetic energy, i.e., those resulting from the final simulation times, range from around 7.0 K up to 10.5 K, the last value occurring for $\langle v_0 \rangle = 300$ m/s. From a 3D wave packet static calculation of a Ne atom doped nanodroplet of 1000 ^4He atoms, we obtained a Ne atom kinetic energy of 17.3 K. Now, taking into account that within the present approximation only one dimension is considered for the Ne motion, we estimate a value of $17.3/3=5.8$ K for the kinetic energy of each coordinate. So that, we infer that when the atomic impurity reaches its limit velocity, there is more kinetic energy corresponding with the zero point energy motion (5.8 K) than purely translational (from 1.2 to 4.7 K).

4. SUMMARY AND CONCLUSIONS

The quantum dynamics of the process of capturing a Ne atom by a superfluid helium nanodroplet formed by 1000 ^4He atoms, $T=0.37$ K, with zero angular momentum has been studied within a TDDFT (helium) + WP (Ne) theoretical framework. Thus, the influence of a rather wide range of neon initial mean velocities (90-1300 m/s) on the dynamics has been explored. To the best of our knowledge this is the first quantum study focused on the pick up dynamics and the motion of the dopant in the nanodroplet and the second more exhaustive analysis of this problem.

The velocities were selected according to the velocity distribution of the neon dopant atom at room temperature ($T=300$ K), which corresponds to a common situation in the pick up chamber

employed in the experiments. For the Ne atom mean velocities equal to 210 m/s and above the atom is always captured by the helium nanodroplet. However, for lower velocities the probability of capture is below the unity (for 90 and 120 m/s is equal to 0.880 and 0.985, respectively) and diminishes as the impinging Ne atom velocity decreases.

The main energy exchange begins with the collision of the atom with the nanodroplet surface. The resulting excess of energy placed in the doped nanodroplet is progressively released by evaporation of some ^4He atoms. The importance of evaporation increases with the initial mean velocity of neon, although only a small percentage of ^4He atoms is evaporated from the nanodroplet. Thus, a maximum value of around 1.5% of evaporated atoms is found for the highest initial mean velocity of neon analyzed (1300 m/s).

The mean value of the Ne atom position inside the nanodroplet follows an oscillatory trajectory, as a result of multiple sequential collisions with the inner surface of the nanodroplet. It has also been observed that, when the Ne atom mean velocity is below the Landau's critical velocity, there is no a net force acting on the atom and due to this its mean velocity remains constant. This is probably the common behavior for nanodroplets which include a bulk-like zone if moderate collision energies are involved, i.e., similar to the ones considered here. In this situation the only energy exchange that occurs has minor character and takes place when the atom collides with the inner surface and leads to some excitation of the surface modes (ripples) of the nanodroplet.

In the future we hope to be able to investigate the influence of angular momentum on the dynamics of the pick up process using the quantum dynamics theoretical method employed here.

Acknowledgements

This work has been supported by the Spanish Ministry of Science and Innovation (projects refs. CTQ2011-27857-C02-01 and FIS2011-28617-C02-01), and we also want to acknowledge the support from the Autonomous Government of Catalonia (A. V. predoctoral fellowship and projects refs. 2009SGR 17, 2014SGR 25 and XRQTC).

Tables

Table 1. Initial values of the energies (in K) involved in the process.^a

N	$E_{\text{Interac.}}$ Ne-helium	E_{Kin} helium	$E_{\text{Pot+Corr}}$ helium
1000	-0.065	124.51	-5520.0

^a E_{Kin} Ne (K) = 9.74, 17.31, 53.02, 108.2, 300.6, 769.4, 1731.2 and 2031.7
for $\langle v_0 \rangle$ (m/s) = 90, 120, 210, 300, 500, 800, 1200 and 1300, respectively.

Table 2. Final excitation energy per He atom of the nanodroplet.

$\langle v_0 \rangle$ (m/s)	Δe (K)
210	0.09
300	0.15
500	0.28
800	0.33
1200	0.39
1300	0.42

Figure captions

Figure 1. Snapshots showing the temporal evolution of the probability density of the Ne atom wave packet, $\rho_{\text{Ne}} \equiv |\phi_{\text{Ne}}(z_{\text{Ne}})|^2$, and helium density, ρ_{He} , along the z-axis for $\langle v_0 \rangle = 500$ m/s. The system is moving from left to the right with the exception of the last snapshot where the reverse occurs.

Figure 2. Mean value of the Ne atom position as a function of time, for different initial velocities $\langle v_0 \rangle$, as indicated by colors. Smaller simulated time intervals are considered for the lower velocities (90 and 120 m/s) due to the absorption of a fraction of the neon wave packet by the NIP (see text).

Figure 3. Mean value of the velocity as a function of time, for different initial velocities $\langle v_0 \rangle$, as indicated by colors, focusing on the initial part of the collision (subfigure located at the top) and during the travelling of the Ne atom through the nanodroplet (subfigure located at the bottom). The time required for the Ne atom to reach the external surface of the nanodroplet, where $\langle z_{\text{Ne}} \rangle = -25$ Å, is equal to 0.76, 0.83, 1.2, 2.0, 3.3, 4.7, 8.3 and 11.0 ps for $\langle v_0 \rangle = 1300, 1200, 800, 500, 300, 210, 120$ and 90 m/s, respectively.

Figure 4. Trajectories of the mean values of the Ne atom velocity and position, for different initial velocities $\langle v_0 \rangle$ as indicated by colors. The dashed line shows the z value for the pure nanodroplet surface.

Figure 5. Energy per helium atom of the nanodroplet as a function of time, for different initial velocities $\langle v_0 \rangle$ as indicated by colors. The inner panel focus on the initial part of the collision, and the collision time on the nanodroplet surface corresponds to the initial increase of the E/N ratio. The value of this time is reported for each $\langle v_0 \rangle$ in the caption of Figure 3.

Figure 6. Number of helium atoms of the nanodroplet as a function of time, for different initial velocities $\langle v_0 \rangle$ as indicated by colors.

Figures

Figure 1

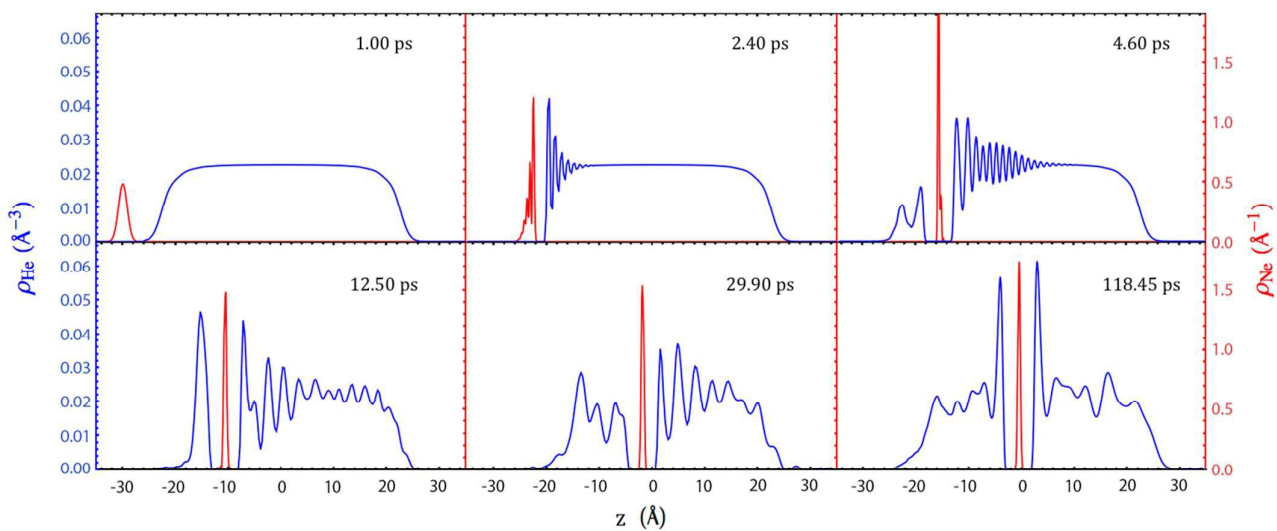


Figure 1. Snapshots showing the temporal evolution of the probability density of the Ne atom wave packet, $\rho_{\text{Ne}} \equiv |\phi_{\text{Ne}}(z_{\text{Ne}})|^2$, and helium density, ρ_{He} , along the z -axis for $\langle v_0 \rangle = 500$ m/s. The system is moving from left to the right with the exception of the last snapshot where the reverse occurs.

Figure 2

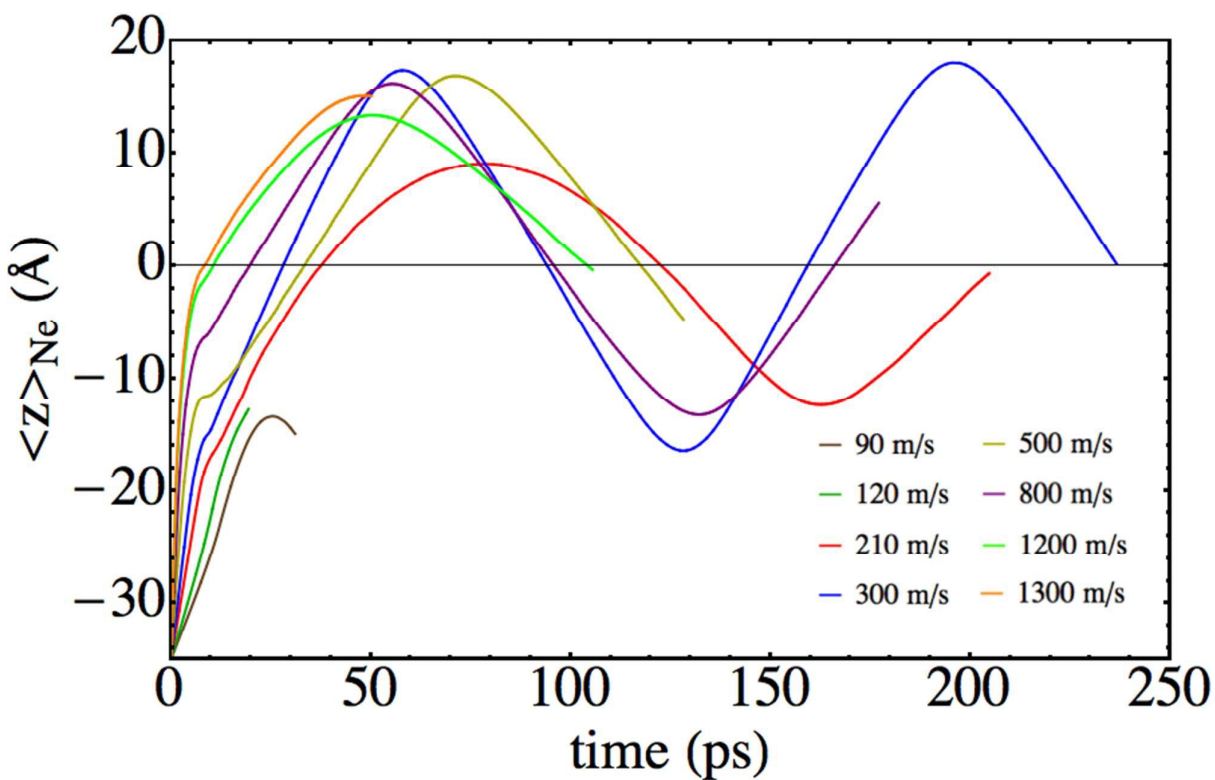


Figure 2. Mean value of the Ne atom position as a function of time, for different initial velocities $\langle v_0 \rangle$, as indicated by colors. Smaller simulated time intervals are considered for the lower velocities (90 and 120 m/s) due to the absorption of a fraction of the neon wave packet by the NIP (see text).

Figure 3

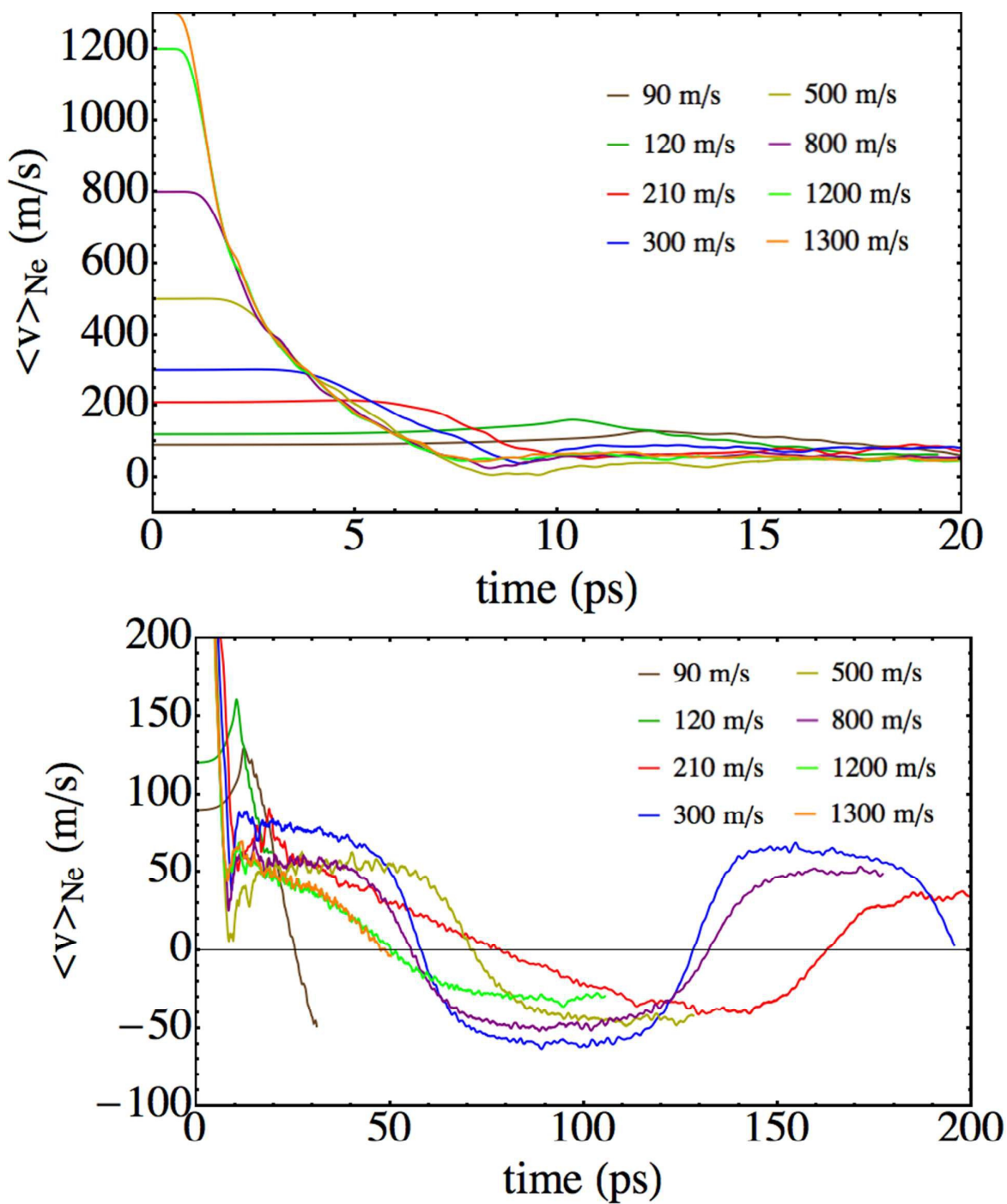


Figure 3. Mean value of the velocity as a function of time, for different initial velocities $\langle v_0 \rangle$, as indicated by colors, focusing on the initial part of the collision (subfigure located at the top) and during the travelling of the Ne atom through the nanodroplet (subfigure located at the bottom). The time required for the Ne atom to reach the external surface of the nanodroplet, where $\langle z_{\text{Ne}} \rangle = -25 \text{ \AA}$, is equal to 0.76, 0.83, 1.2, 2.0, 3.3, 4.7, 8.3 and 11.0 ps for $\langle v_0 \rangle = 1300, 1200, 800, 500, 300, 210, 120$ and 90 m/s , respectively.

Figure 4

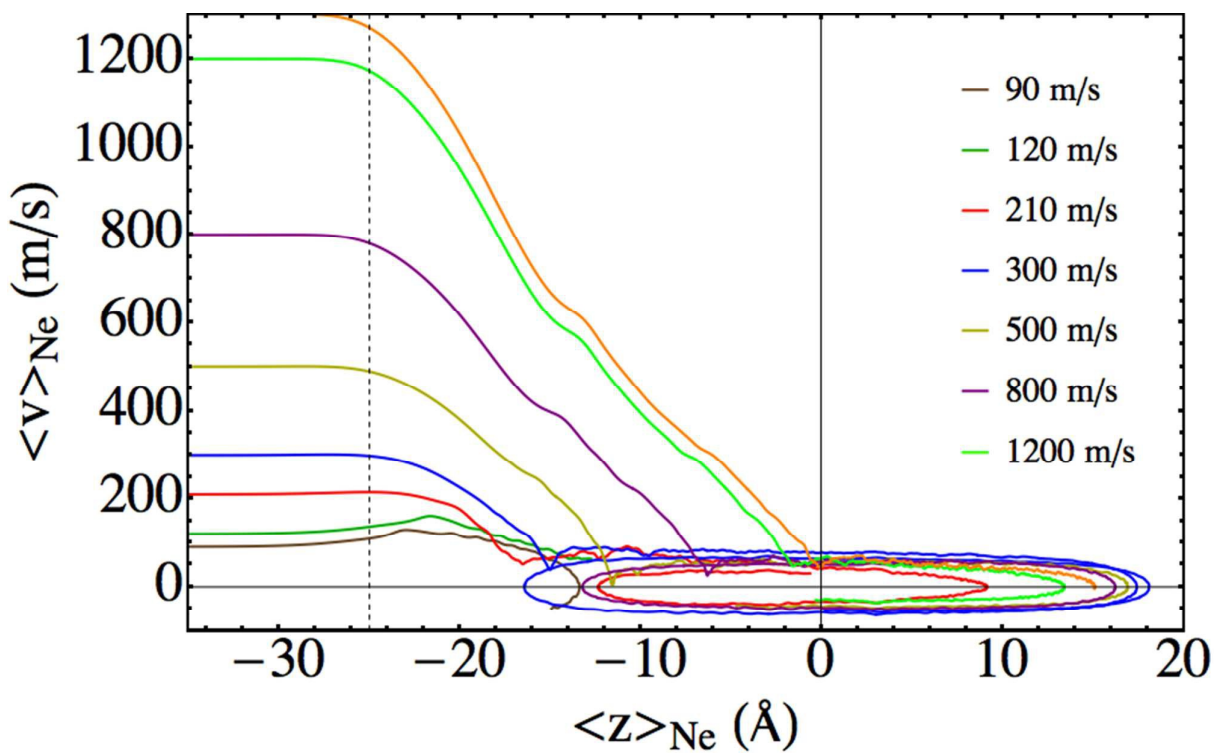


Figure 4. Trajectories of the mean values of the Ne atom velocity and position, for different initial velocities $\langle v_0 \rangle$ as indicated by colors. The dashed line shows the z value for the pure nanodroplet external surface.

Figure 5

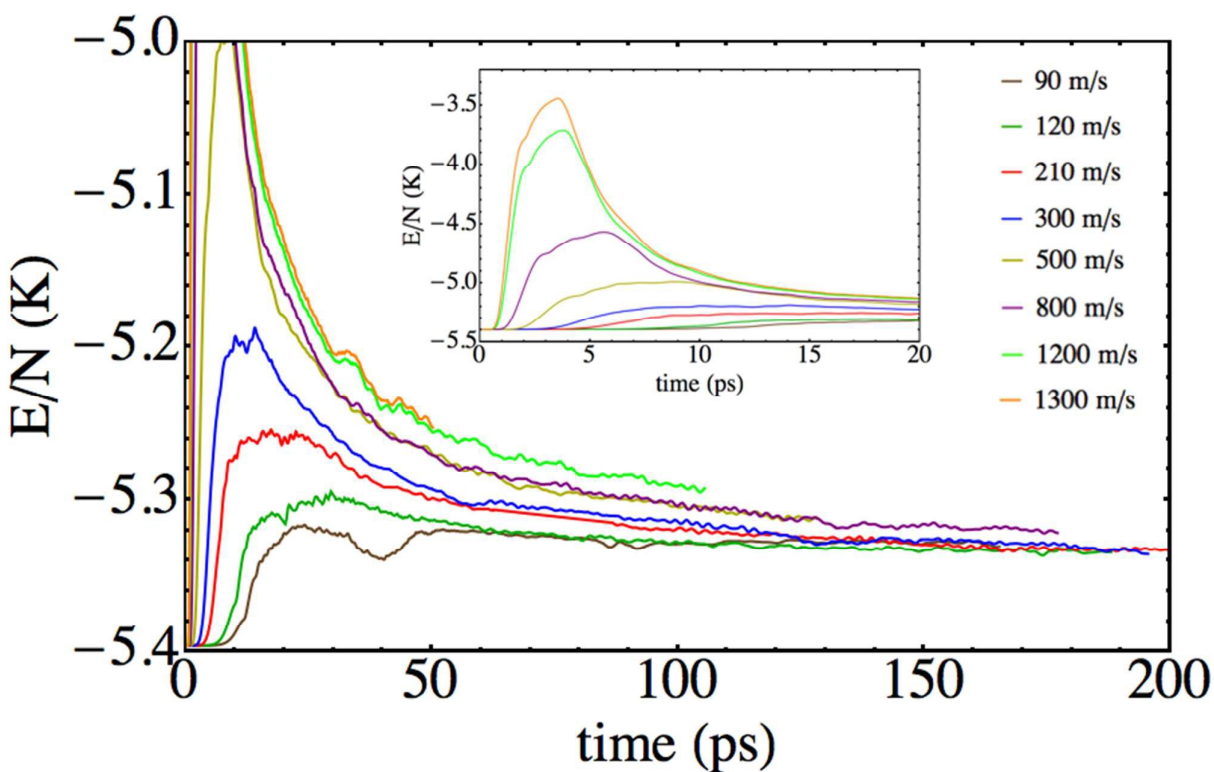


Figure 5. Energy per helium atom of the nanodroplet as a function of time, for different initial velocities $\langle v_0 \rangle$ as indicated by colors. The inner panel focus on the initial part of the collision, and the collision time on the nanodroplet external surface corresponds to the initial increase of the E/N ratio. The value of this time is reported for each $\langle v_0 \rangle$ in the caption of Figure 3.

Figure 6

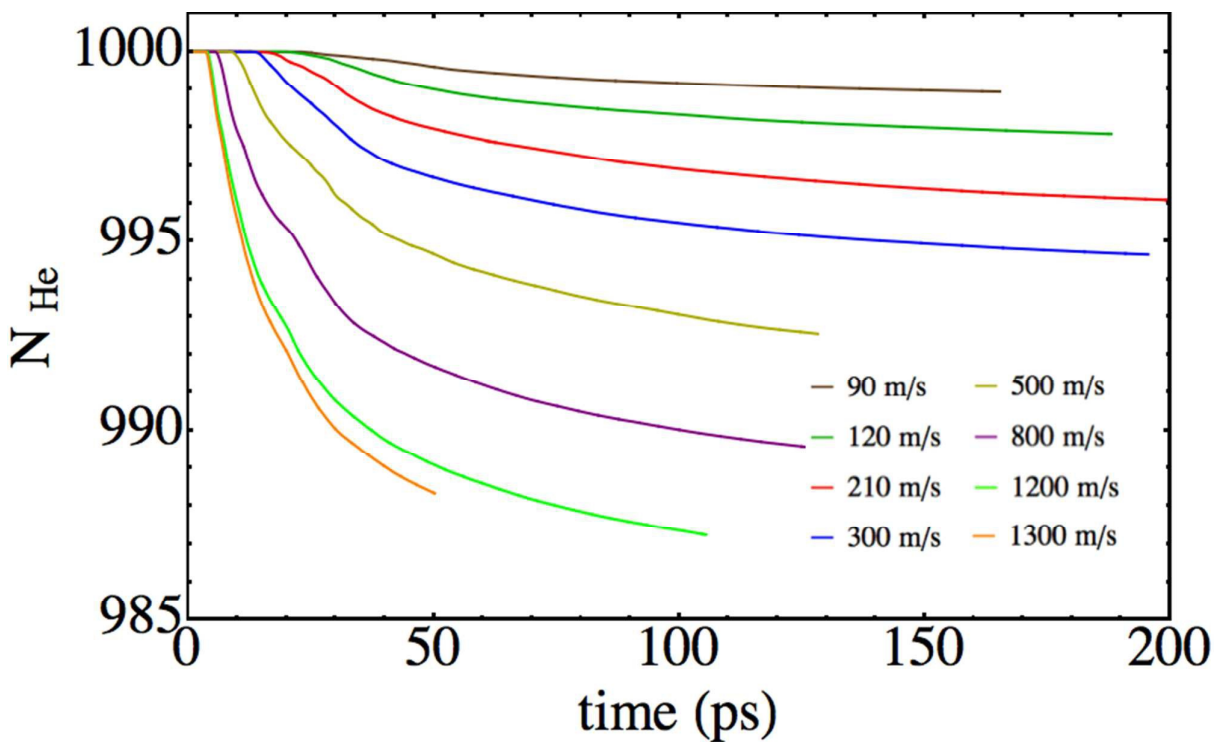


Figure 6. Number of helium atoms of the nanodroplet as a function of time, for different initial velocities $\langle v_0 \rangle$ as indicated by colors.

References

- ¹ J. P. Toennies and A. F. Vilesov, *Angew. Chem. Int. Ed.*, 2004, **43**, 2622-2648.
- ² M. Barranco, R. Guardiola, S. Hernández, R. Mayol, J. Navarro and M. Pi, *J. Low Temp. Phys.*, 2006, **142**, 1-81.
- ³ S. Goyal, D. L. Schutt and G. Scoles, *Phys. Rev. Lett.* 1992, **69**, 933-936.
- ⁴ M. Hartmann, R. E. Miller, J. P. Toennies and A. F. Vilesov, *Science*. 1996, **272**, 1631-1634.
- ⁵ A. Vilà, M. González, R. Mayol and M. Paniagua, *RSC Adv.* 2014, **4**, 44972-44979.
- ⁶ E. Lugovoj, J. P. Toennies and A. F. Vilesov, *J. Chem. Phys.* 2000, **112**, 8217-8220.
- ⁷ G. E. Douberly and R. E. Miller, *J. Phys. Chem. B*, 2003, **107**, 4500-4507.
- ⁸ S. A. Krasnokutski and F. Huisken, *J. Phys. Chem. A.*, 2011, **115**, 7120-7126.
- ⁹ S. Yang and A. M. Ellis, *Chem. Soc. Rev.* 2013, **42**, 472-484.
- ¹⁰ A. Vilà, M. González and R. Mayol, *J. Chem. Theory Comput.*, 2015, **11**, 899-906.
- ¹¹ A. Vilà, M. González and R. Mayol, *Phys. Chem. Chem. Phys.*, accepted 2 November 2015.
- ¹² J. Tiggesbäumker and F. Stienkemeier, *Phys. Chem. Chem. Phys.*, 2007, **9**, 4748-4770.
- ¹³ T. Döppner, T. Diederich, S. Göde, A. Przystawik, J. Tiggesbäumker and K.-H. Meiwes-Broer, *J. Chem. Phys.*, 2007, **126**, 244513.
- ¹⁴ S. Yang, A. M. Ellis, D. Spence, C. Feng, A. Boatwright, E. Latimer and C. Binns, *Nanoscale*. 2013, **5**, 11545-11553.
- ¹⁵ L. F. Gomez, E. Loginov and A. F. Vilesov, *Phys. Rev. Lett.*, 2012, **108**, 155302.
- ¹⁶ E. Latimer, D. Spence, C. Feng, A. Boatwright, A. M. Ellis and S. Yang, *Nano Lett.* 2014, **14**, 2902-2906.
- ¹⁷ A. Slenczka and J. P. Toennies, in *Low Temperature and Cold Molecules*, ed. I. W. M. Smith, Imperial College Press, London, 2008, pp. 345-392 and references cited therein.
- ¹⁸ A. Braun and M. Drabbels, *J. Chem. Phys.*, 2007, **127**, 114303.
- ¹⁹ A. Braun and M. Drabbels, *J. Chem. Phys.*, 2007, **127**, 114304.

-
- ²⁰ A. Braun and M. Drabbels, *J. Chem. Phys.*, 2007, **127**, 114305.
- ²¹ S. A. Krasnokutski and F. Huisken, *J. Phys. Chem. A*, 2010, **114**, 7292–7300.
- ²² T. Takayanagi and M. Shiga, *Chem. Phys. Lett.*, 2003, **372**, 90-96.
- ²³ A. Scheidemann, J. P. Toennies and J. A. Northby, *Phys. Rev. Lett.*, 1990, **64**, 1899-1902.
- ²⁴ M. Lewerenz, B. Schilling, and J. P. Toennies, *J. Chem. Phys.*, 1995, 102, 8191-8207.
- ²⁵ F. F. da Silva, P. Bartl, S. Denifl, O. Echt, T. D., Märk and P. Scheier, *Phys. Chem. Chem. Phys.*, 2009, **11**, 9791-9797.
- ²⁶ H. Schoebel, P. Bartl, C. Leidlmair, S. Denifl, O. Echt, T. D. Maerk, and P. Scheier, *Eur. Phys. J. D*, 2011, **63**, 209-214.
- ²⁷ M. Ratschek, M. Koch and W. E. Ernst, *J. Chem. Phys.*, 2012, **136**, 104201.
- ²⁸ F. Lindebner, A. Kautsch, M. Koch and W. E. Ernst, *Int. J. Mass Spectrom.*, 2014, **365-366**, 255-259.
- ²⁹ P. L. Raston, J. Agarwal, J. M. Turney, H. F. Schaefer III and G. E. Doublerly, *J. Chem. Phys.*, 2013, **138**, 194303.
- ³⁰ T. Premke, E.-M. Wirths, D. Pentlehner, R. Riechers, R. Lehnig, A. Vdovin and A. Slenczka, *Front. Chem.*, 2014, **2**, 51.
- ³¹ H. Schöbel, C. Leidlmair P. Bartl, S. Denifl, T. D. Märk, O. Echt and P. Scheier, *J. Phys.: Conf. Ser.*, 2012, **388**, 012044.
- ³² A. Scheidemann, B. Schilling, J. P. Toennies, and J. A. Northby, *Phys. B*, 1990, **165**, 135-36.
- ³³ M. Lewerenz, B. Schilling and J. P. Toennies, *J. Chem. Phys.*, 1995, **102**, 8191-8207.
- ³⁴ D. Eichenauer, A. Scheidemann and J.P. Toennies, *Z. Phys. D*, 1988, **8**, 295-304.
- ³⁵ J. P. Toennies and A. F. Vilesov, *Chem. Phys. Lett.*, 1995, **235**, 596-603.
- ³⁶ K. K. Lehmann, *Mol. Phys.*, 1999, **97**, 645-666.
- ³⁷ E. Krotscheck and R. Zillich, *Phys. Rev. B*, 1998, **58**, 5707-5718.
- ³⁸ E. Krotscheck and R. Zillich, *Eur. Phys. J. D*, 2007, **43**, 113-116.

-
- ³⁹ E. Krotscheck and R. Zillich, *Phys. Rev. B*, 2008, **77**, 094507.
- ⁴⁰ A. Leal, D. Mateo, A. Hernando, M. Pi and M. Barranco, *Phys. Chem. Chem. Phys.*, 2014, **16**, 23206-23213.
- ⁴¹ F. Dalfovo, A. Lastrì, L. Pricauptenko, S. Stringari and J. Treiner, *Phys. Rev. B*, 1995, **52**, 1193-1209.
- ⁴² N. B. Brauer, S. Smolarek, E. Loginov, D. Mateo, A. Hernando, M. Pi, M. Barranco, W. J. Buma and M. Drabbels, *Phys. Rev. Lett.*, 2013, **111**, 153002.
- ⁴³ D. Mateo, A. Hernando, M. Barranco, E. Loginov, M. Drabbels and M. Pi, *Phys. Chem. Chem. Phys.*, 2013, **15**, 18388-18400.
- ⁴⁴ D. Mateo, F. Gonzalez and J. Eloranta, *J. Phys. Chem. A*, 2015, **119**, 2262-2270.
- ⁴⁵ Some static calculations have been done in order to obtain the width of the wave packet of the Ne atom inside the helium nanodroplet, obtaining a rather small value. This suggests that our approach is realistic enough.
- ⁴⁶ S. M. Cybulski and R. R. Toczyłowski, *J. Chem. Phys.*, 1999, **111**, 10520-10528.
- ⁴⁷ A. Ralston, in *Mathematical Methods for Digital Computers*, eds. A. Ralston and H. S. Wilf, John Wiley & Sons, New York, 1960; Vol. 1, pp 95-109.
- ⁴⁸ R. J. Thompson, *Commun. ACM*. 1970, **13**, 739-740.
- ⁴⁹ M. Frigo, and S. G. Johnson, *IEE Proceedings*, 2005, **93**, 216-231.
- ⁵⁰ A. Vibók and G. G. Balint-Kurti, *J. Phys. Chem.*, 1992, **96**, 8712-8719.
- ⁵¹ D. R. Tilley and J. Tilley, *Condensates and Excitations. Superfluidity and Superconductivity*, Institut of Physics Publishing, Bristol, 1990, pp 41-53.
- ⁵² J. F. Annet, *Superfluid Helium-4. Superconductivity, Superfluids and Condensates*, Oxford University Press, Oxford, 2004, pp 38-43.
- ⁵³ D. Mateo, A. Leal, A. Hernando, M. Barranco, M. Pi, F. Cargnoni, M. Mella, X. Zhang and M. Drabbels, *J. Chem. Phys.*, 2014, **140**, 131101.

⁵⁴ A. Vilà, Ph. D. Thesis, University of Barcelona (2015).